Brigham Young University
BYU ScholarsArchive

All Theses and Dissertations

2016-08-01

Fundamental Principles of Tremor Propagation in the Upper Limb

Andrew Doran Davidson
Brigham Young University

Follow this and additional works at: https://scholarsarchive.byu.edu/etd

 Part of the Mechanical Engineering Commons

BYU ScholarsArchive Citation

Davidson, Andrew Doran, "Fundamental Principles of Tremor Propagation in the Upper Limb" (2016). *All Theses and Dissertations*. 6509.
https://scholarsarchive.byu.edu/etd/6509

This Thesis is brought to you for free and open access by BYU ScholarsArchive. It has been accepted for inclusion in All Theses and Dissertations by an authorized administrator of BYU ScholarsArchive. For more information, please contact scholarsarchive@byu.edu, ellen_amatangelo@byu.edu.

Fundamental Principles of Tremor Propagation in the Upper Limb

Andrew Doran Davidson

A thesis submitted to the faculty of
Brigham Young University
in partial fulfillment of the requirements for the degree of

Master of Science

Steven K. Charles, Chair
Mark B. Colton
Spencer P. Magleby

Department of Mechanical Engineering

Brigham Young University

August 2016

Copyright © 2016 Andrew Doran Davidson

All Rights Reserved

ABSTRACT

Fundamental Principles of Tremor Propagation in the Upper Limb

Andrew Doran Davidson
Department of Mechanical Engineering, BYU
Master of Science

Although tremor is the most common movement disorder, there exist few effective tremor-suppressing devices, in part because the characteristics of tremor throughout the upper limb are unknown. To clarify, optimally suppressing tremor requires a knowledge of the mechanical origin, propagation, and distribution of tremor throughout the upper limb. Here we present the first systematic investigation of how tremor propagates between the shoulder, elbow, forearm, and wrist. We simulated tremor propagation using a linear, time-invariant, lumped-parameter musculoskeletal model relating joint torques and the resulting joint displacements. The model focused on the seven main degrees of freedom (DOF) from the shoulder to the wrist and included coupled joint inertia, damping, and stiffness. We deliberately implemented a simple model to focus first on the most basic effects. Simulating tremorogenic joint torque as a sinusoidal input, we used the model to establish fundamental principles describing how input parameters (torque location and frequency) and joint impedance (inertia, damping, and stiffness) affect tremor propagation. We expect that the methods and principles presented here will serve as the groundwork for future refining studies to understand the origin, propagation, and distribution of tremor throughout the upper limb in order to enable the future development of optimal tremor-suppressing devices.

Keywords: Essential Tremor, Parkinsons Disease, musculoskeletal dynamics, tremor suppression

ACKNOWLEDGMENTS

The research presented here has been made possible by the numerous people who have guided and supported me throughout the course of my studies. I am grateful for the assistance provided by my committee members, Dr. Colton and Dr. Magleby, as well as the many BYU faculty members that have contributed to my education. I am especially grateful for my adviser, Dr. Charles, whose direction and patience throughout the research process has brought me significant academic and personal growth.

I would also like to express my deep gratitude for my loving wife, Amy, for her continual support and showing genuine interest in my research. Likewise, this research would not have been possible without the constant encouragement and support of my parents, Doran and Diane. I also greatly appreciate the funding received from the National Institutes of Health (NIH Grant R15NS087447, Quantitative Characterization of Essential Tremor for Future Tremor Suppression).

TABLE OF CONTENTS

LIST OF TABLES

LIST OF FIGURES

CHAPTER 1. INTRODUCTION

Tremor is the most common movement disorder [1, 2] and results from an interaction between pathological neural control and the frequency response of the limb [3–5]. The two leading conditions that cause tremor in the upper limb are Essential Tremor and Parkinsons disease. Other conditions that can cause tremor include dystonia, cerebellar ataxia, traumatic brain injury, stroke, and multiple sclerosis [1]. More than 65% of the population with upper limb tremor present serious difficulties performing daily living activities such as eating, buttoning a shirt, writing, etc. [6].

Unfortunately, medication and surgical interventions are only partially effective, and patients have few non-invasive treatment options. For example, the only two medications with unequivocal efficacy in treating Essential Tremor, propranolol (a beta-blocker) and primidone (an anti-convulsant), reduce the tremor by only 50%, and only 50% of patients benefit from one or both of these medications [7, 8]. Patients who do not respond favorably to medication may be eligible for deep brain stimulation (DBS), which provides 55-90% tremor reduction [8] and is effective in 70-90% of patients, though its efficacy is gradually lost in some patients [7]. However, despite its efficacy, DBS is by no means an optimal solution because of its highly invasive nature. Many patients prefer to suffer the debilitating consequences of tremor rather than undergo neurosurgery.

A significant obstacle to developing effective tremor-suppressing devices is that the characteristics of tremor are not known throughout the upper limb. Given the challenges associated with medications and DBS, it is important to give patients non-pharmacological, non-surgical alternatives. Yet there is a surprising lack of effective tremor-suppressing devices. Optimally suppressing tremor requires a knowledge of tremor throughout the upper limb: where in the upper-limb the tremor originates (mechanically), how it propagates, and where it manifests most severely. However, most studies have only investigated tremor in a single degree of freedom (most often either at the endpoint of outstretched arms or in wrist flexion-extension) [9]. Therefore, the origin, propa-

gation, and distribution of tremor are currently unknown, greatly limiting our ability to effectively reduce tremor with tremor-suppressing devices.

The long-term objective of this work is to understand the origin, propagation, and distribution of tremor throughout the upper limb in order to enable the future development of optimal tremor-suppressing devices. Here we present basic principles underlying the propagation of tremor throughout the upper limb. As this is the first systematic investigation of tremor propagation of which we are aware, we deliberately chose a simple model to focus first on the most basic effects. We simulated tremor propagation using a linear time-invariant (LTI), lumped-parameter model of the relationship between joint torques and the resulting joint displacements. The model included the seven main degrees of freedom (DOF) from the shoulder to the wrist and included coupled joint inertia, damping, and stiffness. We used the model to establish the fundamental principles that govern how tremor source parameters (input torque location and frequency) and joint impedance (inertia, damping, stiffness) affect tremor propagation.

CHAPTER 2. METHODS

2.1 Model of Upper Limb Dynamics

2.1.1 Model Development

To establish the most fundamental principles of tremor propagation, we used the simplest possible model between input torques and output displacements that can capture the phenomena of tremor propagation. A linear model was used because previous studies have shown that linear models can effectively capture the key elements of the dynamics of small upper limb movements (such as tremor) [10, 11]. Additionally, tremor consists of relatively small displacements around an equilibrium point and LTI models allow for the use of principles and tools from linear systems theory, including frequency response (see below).

2.1.2 Model Structure

The musculoskeletal dynamics of the upper limb were modeled as $I\ddot{\mathbf{q}}+D\dot{\mathbf{q}}+K\mathbf{q}=\boldsymbol{\tau}$, where $\mathbf{q}=[q_1\ q_2\ q_3\ q_4\ q_5\ q_6\ q_7]^T$ represents angular displacement in each DOF, positive in shoulder flexion (q_1), shoulder adduction (q_2), shoulder internal rotation (q_3), elbow flexion (q_4), forearm pronation (q_5), wrist flexion (q_6), and wrist ulnar deviation (q_7) (Figure 2.1); I, D, and K are 7-by-7 matrices representing the coupled inertia, damping, and stiffness in these DOF, respectively; and $\boldsymbol{\tau}=[\tau_1\ \tau_2\ \tau_3\ \tau_4\ \tau_5\ \tau_6\ \tau_7]^T$ represents the input torque (arising from muscle activity) acting on each DOF.

The off-diagonal elements of the impedance matrices determine system coupling. Off-diagonal elements of the 7-by-7 inertia matrix (products of inertia) are not intuitive or easily predicted. Consequently, the non-zero values of the inertia matrix were determined by the RVC Toolbox, which leveraged the iterative Newton-Euler method to calculate the posture specific inertia matrix. Stiffness is due to muscle stretch, at least when motion is not near the extreme ends of the

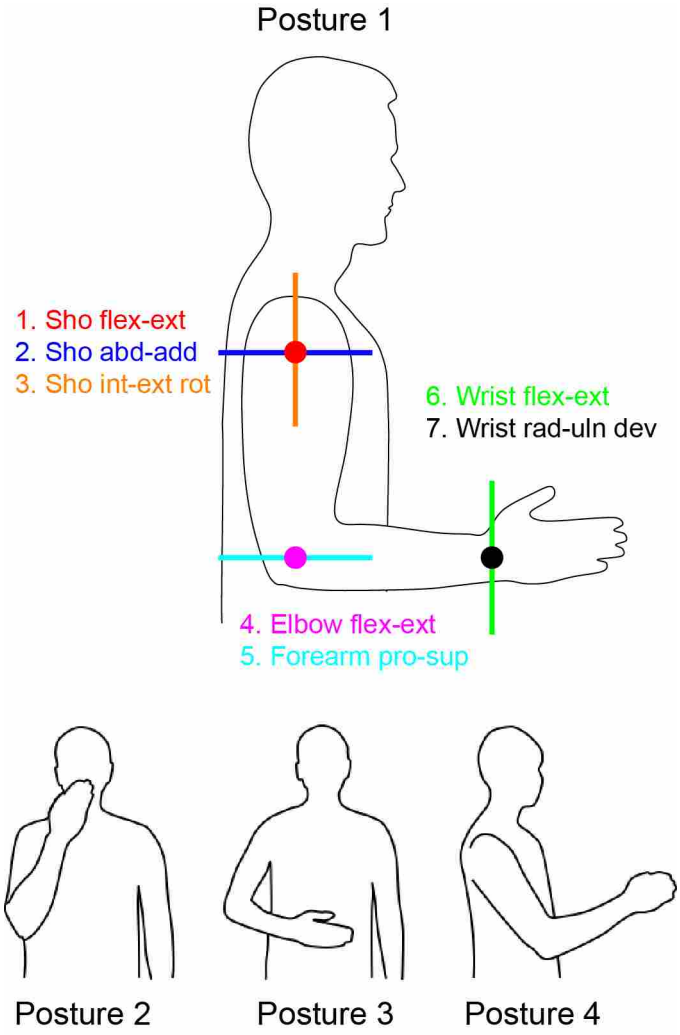

Figure 2.1: Degrees of freedom (DOF) and postures included in the study. The model of the upper limb included seven DOF, designated by their like-colored axes of rotation: Shoulder flexion-extension, shoulder abduction-adduction, shoulder internal-external rotation, elbow flexion-extension, forearm pronation-supination, wrist flexion-extension, and wrist radial-ulnar deviation. This order (1-7) and color scheme is used throughout the paper. Posture 1 is the default posture and is identical to anatomical position except that the elbow is flexed 90 and the forearm is midway between supination and pronation. Postures 2-4 were used as a sample of postures from daily life to investigate the sensitivity of tremor propagation to changes in posture. Posture 2 places the hand in front of the mouth and represents feeding and grooming activities. In Posture 3 the hand is in the workspace in front of the abdomen and represents many activities of daily living requiring fine manipulation, such as opening items or writing. Posture 4 represents reaching tasks. The joint angles for each posture are given in Table 2.3.

joint range of motion. Coupling in the 7-by-7 stiffness matrix is due to multi-articular muscles. Based on our knowledge of muscle origin and insertion points, we can predict which DOF are coupled by multi-articular muscles, and therefore whether the off-diagonal elements of the stiffness matrix are non-zero (coupled) or zero (uncoupled), as shown in Table 2.1. However, some DOF share multi-articular muscles but may experience weak or even negligible coupling, for example because the muscle moment arms are small. In practice the degree of coupling was determined by prior experiments that measured the values of off-diagonal matrix elements. For elements that have not been measured, we tested a wide variety of plausible values. Damping is also due to muscle stretching like stiffness. Therefore, the pattern of zero and non-zero values in the damping matrix follows that of the stiffness matrix.

Table 2.1: Stiffness matrix values predicted to be non-zero (X), zero or negligible (0), and those that are not easily predicted (?). The abbreviations represent shoulder flexion-extension (SFE), shoulder abduction-adduction (SAA), shoulder internal-external rotation (SEIR), elbow flexion-extension (EFE), forearm pronation-supination (FPS), wrist flexion-extension (WFE), and wrist radial-ulnar deviation (WRUD).

	Stiffness Matrix						
	SFE	**SAA**	**SIER**	**EFE**	**FPS**	**WFE**	**WRUD**
SFE	X	X	X	X	?	0	0
SAA	X	X	X	?	?	0	0
SIER	X	X	X	?	?	0	0
EFE	X	?	?	X	?	?	?
FPS	?	?	?	?	X	X	X
WFE	0	0	0	?	X	X	X
WRUD	0	0	0	?	X	X	X

2.1.3 Model Parameters

The full 7-by-7 inertia, damping, and stiffness matrices are not available in the literature, so they were assembled from prior studies that measured portions of the matrices (Table 2.2). Please note that although values were estimated as accurately as possible, the exact values are not critical

because we also performed a thorough sensitivity analysis to determine the effect of uncertainty in our matrix values.

Inertia: Prior measurements of inertial values for individual body segments were used in conjunction with the Robotics Vision and Control (RVC) toolbox to calculate the full inertia matrix, including coupling between segments. More specifically, the body-segment inertial parameters were taken from previous studies [12] using values for a 50^{th} percentile male. The coupled inertia matrix was calculated for different postures (see below) via Denavit-Hartenberg (DH) parameters using the RVC toolbox (Figure 2.2, Table 2.3) [13, 14].

Stiffness: We started with purely passive stiffness (in the absence of muscle activity) but later added active stiffness to model co-contraction (see below). The diagonal and off-diagonal values corresponding to planar shoulder-elbow movements were taken from the torque-dependent regression by [15], with zero torque for passive stiffness. To estimate the remaining diagonal and off-diagonal elements of the sub-matrix for the shoulder and elbow, we scaled a recent measurement of passive stiffness in the 3 DOF of the shoulder [16] to match the values from [15]. The 3-by-3 sub-matrix representing wrist and forearm stiffness was taken from [17]. The unknown off-diagonal stiffness representing coupling between the shoulder-elbow and the forearm-wrist systems were initially assumed zero but then changed to a variety of non-zero values in the sensitivity analysis. Many studies have shown joint stiffness to be nearly symmetric [17–20]. To simplify the analysis, we used in our simulations only the symmetric part of the stiffness matrix, calculated as the average of the matrix and its transpose.

Damping: Only few elements of the 7-by-7 damping matrix have been measured. However, several past shoulder-elbow studies have found the shape and orientation of the damping and stiffness ellipses to be similar [21–23], indicating that the matrices are roughly proportional (the shape and orientation of an ellipse represent the relative magnitudes of the matrix elements). Therefore, some past studies involving few DOF have approximated the damping matrix to be proportional to the stiffness matrix, the proportionality constant chosen so the new matrix would match past measurements of individual matrix elements or damping ratios [24, 25]. However, our 7-by-7 matrix involves different sets of multi-articular muscles, and it became clear that a single constant of proportionality was unable to match previously measured damping ratios. Therefore, we used one constant of proportionality (0.07 s) for the 4-by-4 submatrix representing the shoulder-elbow

system, and a different constant of proportionality (0.028 s) for the 3-by-3 submatrix representing the forearm-wrist system. The other off-diagonal values are unknown and were initially assumed zero but later varied through a range of non-zero values in the sensitivity analysis. Using two different constants of proportionality allowed shoulder-elbow damping and forearm-wrist damping to be proportional to shoulder-elbow stiffness and forearm-wrist stiffness, respectively, and for the range of the resulting single-DOF damping ratios (0.18-0.42) to match the range measured previously (0.14-0.48) [22, 26–28].

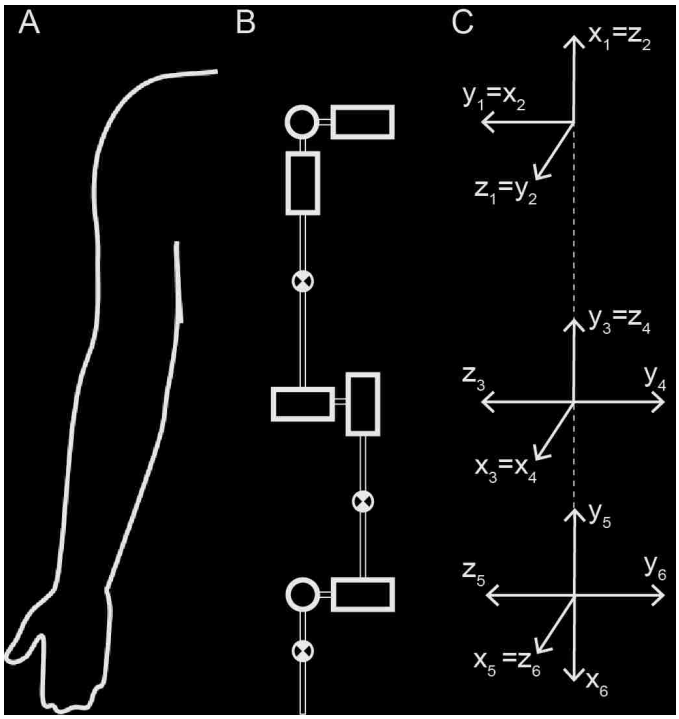

Figure 2.2: Kinematic description of the upper limb using the Denavit-Hartenberg (DH) convention. To calculate the full, coupled inertia matrix, we modeled the seven main degrees of freedom of the shoulder, elbow, forearm, and wrist as revolute joints (A-B) and converted the model to DH parameters (Table 2.3) using the intermediate coordinate frames defined in C. Adapted from [29].

2.1.4 Input-Output Relationships

Our model has seven inputs (a torque in each DOF) and seven outputs (a displacement in each DOF). In such a multiple-input, multiple-output model, every input has the potential to affect every output. The relationships between inputs and outputs are given by transfer functions, derived

Table 2.2: Joint inertia, damping, and stiffness matrices used for basic simulations involving posture 1. For each matrix, element ij (row, column) represents the change in torque in DOF i associated with a change in acceleration, velocity, or position in DOF j.

Inertia (kg m2)							
	SFE	**SAA**	**SIER**	**EFE**	**FPS**	**WFE**	**WRUD**
SFE	0.269	0	0	0.076	0	0	-0.014
SAA	0	0.196	0.083	0	-0.002	0.009	0
SIER	0	0.083	0.079	0	0	0.011	0
EFE	0.076	0	0	0.076	0	0	-0.012
FPS	0	-0.002	0	0	0.002	0	0
WFE	0	0.009	0.011	0	0	0.003	0
WRUD	-0.014	0	0	-0.012	0	0	0.003

Damping (Nms/rad)							
	SFE	**SAA**	**SIER**	**EFE**	**FPS**	**WFE**	**WRUD**
SFE	0.756	0.184	0.02	0.187	0	0	0
SAA	0.184	0.383	0.267	0	0	0	0
SIER	0.02	0.267	0.524	0	0	0	0
EFE	0.187	0	0	0.607	0	0	0
FPS	0	0	0	0	0.021	0.001	0.008
WFE	0	0	0	0	0.001	0.028	-0.003
WRUD	0	0	0	0	0.008	-0.003	0.082

Stiffness (Nm/rad)							
	SFE	**SAA**	**SIER**	**EFE**	**FPS**	**WFE**	**WRUD**
SFE	10.8	2.626	0.279	2.67	0	0	0
SAA	2.626	5.468	3.821	0	0	0	0
SIER	0.279	3.821	7.486	0	0	0	0
EFE	2.67	0	0	8.67	0	0	0
FPS	0	0	0	0	0.756	0.018	0.291
WFE	0	0	0	0	0.018	0.992	-0.099
WRUD	0	0	0	0	0.291	-0.099	2.92

Table 2.3: DH parameters for each posture. Together with Figure 2.2C, the angle value (θ_i), link offset (d_i), link length (a_i), and link twist (α_i) fully define each posture. Parameters L_{ua}, L_{fa}, and L_h refer to the lengths of the upper arm, forearm, and hand, respectively.

	DH Parameters			
	θ_i	d_i	a_i	α_i
Link 1	$\theta_1 - \pi/2$	0	0	$\pi/2$
Link 2	$\theta_2 + \pi/2$	0	0	$\pi/2$
Link 3	$\theta_3 + \pi/2$	$-L_{ua}$	0	$\pi/2$
Link 4	θ_4	0	0	$-\pi/2$
Link 5	θ_5	$-L_{fa}$	0	$\pi/2$
Link 6	$\theta_6 - \pi/2$	0	0	$-\pi/2$
Link 7	θ_7	0	$-L_h$	0

	Posture 1	Posture 2	Posture 3	Posture 4
$\boldsymbol{\theta_1}$	0	$\pi/4$	$\pi/8$	$\pi/8$
$\boldsymbol{\theta_2}$	0	0	0	0
$\boldsymbol{\theta_3}$	0	$\pi/4$	$\pi/4$	$\pi/4$
$\boldsymbol{\theta_4}$	$\pi/2$	$3\pi/4$	$\pi/2$	$\pi/4$
$\boldsymbol{\theta_5}$	$\pi/2$	$\pi/4$	$\pi/4$	$\pi/4$
$\boldsymbol{\theta_6}$	0	$\pi/4$	$\pi/4$	$\pi/4$
$\boldsymbol{\theta_7}$	0	$-\pi/8$	$-\pi/8$	$-\pi/8$

as follows [30]. The model $I\ddot{\mathbf{q}} + D\dot{\mathbf{q}} + K\mathbf{q} = \boldsymbol{\tau}$ can be transformed into the Laplace domain as $(Is^2 + Ds + K)\mathbf{Q}(s) = \mathbf{T}(s)$, where $\mathbf{Q}$ and $\mathbf{T}$ are the Laplace transforms of $\mathbf{q}$ and $\boldsymbol{\tau}$, respectively, and s is the Laplace variable. Summarizing $Is^2 + Ds + K$ as $\mathbf{Z}(s)$ and solving for $\mathbf{Q}$ yields $\mathbf{Q} = Z^{-1}\mathbf{T}$. Defining the transfer function matrix $G(s)$ as Z^{-1} yields $\mathbf{Q} = G\mathbf{T}$. G is a 7-by-7 matrix with 49 transfer functions, one for each input-output relationship, i.e. $Q_{i/k} = G_{ik}T_k$, where $Q_{i/k}$ is the output in DOF i due to an input in DOF k. Each transfer function has the same 14^{th} order denominator, but generally different numerators. The total output at each DOF is a linear combination of the inputs at each DOF, the weights of the linear combination being the transfer functions associated with that output: $\sum_{k=1}^{7} G_{ik}T_k$.

Note that because our impedance matrices are symmetric, the transfer function matrix is symmetric. Human joint impedance is roughly symmetric; inertia is symmetric by definition [31], and many studies have shown joint stiffness to be nearly symmetric [17–19]. In our model I, D, and K are perfectly symmetric, so Z is symmetric, and consequently G as well (the inverse of a symmetric matrix is symmetric). Therefore, $G_{ik} = G_{ki}$, or $\frac{Q_{i/k}(s)}{T_k(s)} = \frac{Q_{k/i}(s)}{T_i(s)}$. If the inputs are equal,

$q_{i/k}(t) = q_{k/i}(t)$. In other words, the response in DOF i to an input in DOF k is the same as the response in DOF k to an equal input in DOF i . As a corollary, the responses in all DOF due to an input in DOF i are the same as the individual responses in DOF i due to equal inputs in all DOF.

2.1.5 Frequency Response

If the inputs are sinusoidal, the relationships between inputs and outputs can be specified in terms of magnitude ratios and phase shifts. If the input in DOF k is $\tau_k(t) = A_k sin(\omega_k t + \phi_k)$, it can be shown [30] that the steady-state output in DOF i is also sinusoidal: $q_{i/k}(t) = M_{ik}A_k sin(\omega_k t + \phi_k + \phi_{ik})$, with the same frequency (ω_k) but amplitude $M_{ik}A_k$ and phase shift ϕ_{ik} relative to the input. M_{ik} is the ratio of the output magnitude over the input magnitude (called magnitude ratio) and can be calculated from the transfer function as a function of the input frequency: $M_{ik}(\omega_k) = |G_{ik}(j\omega_k)|$, where $j = \sqrt{-1}$. Likewise, the phase shift ϕ_{ik} can be computed from the transfer function as a function of the input frequency: $\phi_{ik}(\omega_k) = \angle G_{ik}(j\omega_k)$ [30]. The total output in DOF i is a linear combination of the individual outputs: $q_i(t) = \sum_{k=1}^{7} M_{ik}A_k sin(\omega_k t + \phi_k + \phi_{ik})$ [32].

If the sinusoidal inputs are equal, the relationships between inputs and outputs can be specified in terms of a single magnitude ratio and phase shift. To simplify and place all DOF on equal footing (see Discussion), we assumed equal input torques in all DOF: $\tau_k(t) = Asin(\omega t)$ for all k. The output then becomes $q_i(t) = A\sum_{k=1}^{7} M_{ik} sin(\omega t + \phi_{ik})$, which is itself a sinusoid: $q_i(t) = AM_i sin(\omega t \phi_i)$. The magnitude ratio M_i and phase shift ϕ_i can be calculated as the magnitude and direction of the vector sum of the k individual vectors (phasors) of magnitude M_{ik} and direction ϕ_{ik}. In practice, M_i and ϕ_i are more easily calculated from the transfer function matrix as follows. Since all inputs are equal, the expression for Q_i above can be written as $Q_i = [\sum_{k=1}^{7} G_{ik}]T = G_i T$. The magnitude ratio and phase shift can be calculated from G_i as $M_i(\omega) = |G_i(j\omega)|$ and $\phi_i(\omega) = \angle G_i(j\omega)$. Thus the output q_i due to multiple inputs of equal frequency, amplitude, and phase is specified by the magnitude ratio and phase shift of the sum of the transfer functions G_{ik} associated with output i [33].

2.2 Simulation Protocol

To investigate how tremor propagates, we injected sinusoidal torque inputs into various DOF and observed the resulting displacement in each DOF. To simplify and place all DOF on equal footing, we assumed torque inputs in all DOF had equal amplitude, frequency, and phase (see Discussion). Simulations were performed systematically in increasing levels of model complexity, starting with a single input and building up to inputs in all seven DOF. Using this approach, we investigated the following six questions.

1) Where do tremor frequencies fall on the frequency response of the upper limb? Tremors occur most frequently at frequencies between 4 and 12 Hz [34], which we called the tremor band. As an underdamped low-pass filter, the upper limb passes input torques of low frequency, amplifies torques of intermediate frequency, and reduces torques of high frequency. To understand what it does to input torques in the tremor band, we investigated the frequency response of the upper limb in the tremor band, focusing in particular on 4, 8, and 12 Hz.

2) Does tremor propagate mostly because of inertial, damping, or stiffness coupling? Tremor propagates because the off-diagonal elements of the inertia, damping, and stiffness matrices couple the DOF. Does one of these matrices cause most of the coupling? To answer this question, we ran simulations with and without the diagonal elements of these matrices.

3) Does tremor spread to all DOF, or does it focus in certain DOF? The coupling between DOF spreads the tremor, but the spreading may be narrow or broad (i.e. to few or many DOF, respectively).

4) Does tremor propagation change from proximal to distal? Prior studies have found proximal-distal differences in movement characteristics due to differences in impedance [24, 25]. Do these differences in impedance cause differences in tremor propagation as well?

Prior experimental studies have investigated the effect of increasing impedance on tremor [2, 35–43]. We simulated these effects with the following questions.

5) How does inertial loading affect tremor propagation? We simulated inertial loading by scaling the entire inertia matrix by a factor ranging from 1.0 to 3.0, in increments of 0.2.

6) How does viscoelastic loading affect tremor propagation? Increasing the viscoelasticity of the limb can occur through bracing or muscle contraction. Bracing the upper limb may increase stiffness, damping, or both. Common commercially available wrist braces increase wrist

stiffness by a factor of roughly 1.8 [44], but custom-made braces could be significantly stiffer. To represent a range of possible braces, we increased only stiffness, only damping, and both stiffness and damping, all by factors ranging from 1.0 to 10.0, in increments of 0.5. Muscle contraction increases stiffness in proportion to muscle torque, but it increases damping in proportion to the square root of muscle torque, leaving the damping ratio approximately constant [15, 22]. We simulated co-contraction by increasing the stiffness matrix by a factor of 1-10 (in increments of 0.5) and the damping matrix by the square root of that factor. Prior measurements of stiffness in wrist flexion-extension during torque production have found that a 1-10 increase in stiffness are associated with torques from 0 to 2.1 Nm [45–47], which is about 27% of the maximum voluntary torque in wrist FE [48].

2.3 Data Processing and Analysis

Since the input torques were sinusoidal, the output displacement in each DOF was specified in terms of magnitude ratio and phase shift (see Frequency Response). More specifically, we transformed our model into state space form, determined the transfer function matrix, and computed the magnitude ratio and phase shift using Matlabs *ss*, *tf*, and *bode* functions, respectively.

To present the results, we plotted the magnitude ratio and phase shift separately as functions of input frequency (frequency response plots), the magnitude ratio and phase shift combined at a specific input frequency (phasor plots), or the magnitude ratio at a specific input frequency as a function of DOF (to demonstrate the magnitude of coupling between DOF). In phasor plots, the magnitude and angle of each phasor represent the magnitude ratio and phase shift of a particular input-output relationship. The total output in a given DOF is the vector sum of the individual phasors, so phase plots allow one to visualize if the individual outputs in a given DOF (caused by inputs at different DOF) add constructively or destructively.

2.4 Sensitivity Analysis

To determine the effect of uncertainty in our model parameters and test the robustness of our results, we repeated the simulations with variations in inertia, damping, and stiffness. First, we tested inertia, damping, and stiffness matrices at half and twice their original values, scaled

individually and in combinations. Second, we tested the sensitivity of our results to individual matrix elements by calculating at 4, 8, and 12 Hz the slope of the magnitude ratio with respect to each element of each impedance matrix. The slope was computed as the difference derivative from 0.9 to 1.1 times the original value of the matrix element. We identified the most sensitive matrix elements as those with a slope magnitude greater than 0.1 (meaning that multiplying or dividing this matrix element by x increased or decreased the magnitude ratio by $0.1x$ or more), and we repeated simulations at half and twice the original value of these individual matrix elements. Third, we replaced the unknown off-diagonal values of the stiffness matrix (initially assumed zero) with values ranging from small (0.01) to very large (the average of the two corresponding diagonal values), including both positive and negative versions of these values. Since the off-diagonal values of the stiffness matrix are usually considerably smaller than the diagonal values, this range in off-diagonal values is likely larger than the actual range. The damping matrix was calculated by scaling the stiffness matrix, as described above. To determine the off-diagonal values of the damping matrix that did not belong to the shoulder-elbow system or the forearm-wrist system, we scaled using an average of the two constants of proportionality. Fourth, to ensure that any proximal-distal differences were not caused by calculating the damping matrix using different constants of proportionality for the shoulder-elbow and forearm-wrist systems, we repeated our simulations using only one constant (either 0.07 or 0.028) for the whole matrix.

To determine the effect of posture on our results, we also repeated our simulations at a variety of postures (Figure 2.1). Changes in posture only affected the inertia matrix. Adjustments to the inertia matrix were calculated by adjusting the DH parameter joint angle values (θ) of each DOF for each posture (Table 2.3). The stiffness and damping matrices were modeled as posture-independent since past measurements of postural stiffness have found short-range stiffness to be largely independent of joint angle [49, 50]. The postures in Figure 2.1 were chosen as a sample of the most common postures encountered in activities of daily living. We deliberately avoided postures near the limit of the range of motion, where stiffness and damping change significantly. At each posture, we also tested neighboring postures by varying the angle of each DOF through a range of 15°.

CHAPTER 3. RESULTS

3.1 Simulations

Findings are presented as answers to the six questions posed above (Simulation Protocol).

Where do tremor frequencies fall on the frequency response of the upper limb? The full, coupled 7-DOF system can be characterized by its natural frequencies and damping ratios (which belong to the system and cannot be assigned to individual DOF). The natural frequencies lie below or in the tremor band (0.67, 1.08, 1.60, 1.88, 3.22, 4.86, and 7.04 Hz), with damping ratios ranging from 0.15 to 0.68 (the range mentioned in Methods refers to the damping ratios of individual DOF in isolation, similar to how they were measured). The low damping ratios allow resonance in all DOF, but the distal DOF feel the effects of resonance in the tremor band much more than the proximal DOF. Note that most of the changes in magnitude ratio between DOF occurred at frequencies below the tremor band (Figure 3.1A). Although the magnitude ratio continues to change in the tremor band, lines rarely cross in the tremor band, indicating that the order of output magnitudes is stable in the tremor band. In other words, statements about which DOF have the greatest magnitude ratios are relatively robust for any tremor band frequency. How the individual responses combine in a given DOF depends on the phase shift (Figure 3.1B) as well, since responses may add constructively or destructively (Figure 3.1C).

Does tremor propagate mostly because of inertial, damping, or stiffness coupling? Most of the coupling is inertial—removing the off-diagonal elements of the stiffness and damping matrices only had a minor effect (Figure 3.1D). Because the coupling is mostly inertial, it is somewhat predictable; DOF with parallel axes are coupled (assuming centers of mass are located off-axis). For example, input in shoulder internal rotation affects wrist flexion-extension because their axes are parallel. However, DOF do not need to have parallel axes to affect each other; input in shoulder adduction produces tremor in shoulder internal rotation and wrist flexion, neither of which have axes parallel to shoulder adduction.

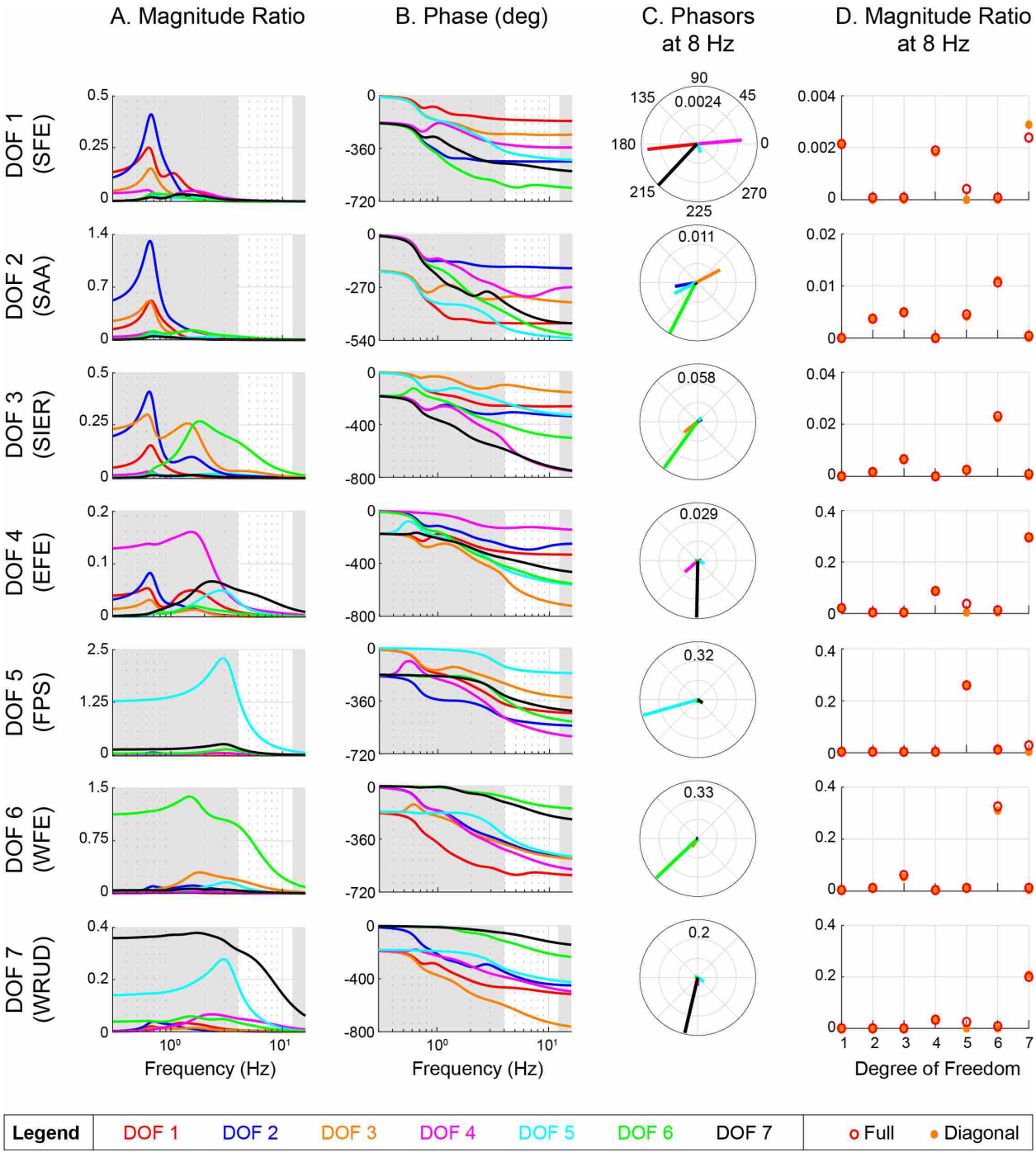

Figure 3.1: Frequency response of all input-output relationships. Row i presents the frequency response for an input in DOF i (row label) and output in DOF k (color—see legend). Because the transfer function matrix is symmetric, row i also presents the frequency response for an input in DOF k (color—see legend) and output in DOF i (row label).

Figure 3.1: (Caption continued) A. Magnitude ratio, which is the ratio of magnitude of the output (tremor) over the magnitude of the input (torque). The tremor band (4-12 Hz) is emphasized in white. B. Phase shift of the output relative to the input. C. Phasor plots for an input frequency of 8 Hz. The magnitude and phase of each phasor (vector) is the same as the magnitude ratio and phase shift of the like-colored lines (on the same row), evaluated at 8 Hz. These plots demonstrate how multiple outputs add constructively or destructively depending on their phase, and that a single phasor dominates for most DOF. The number at the top of plot is the magnitude ratio at the outer-most circle. D. Magnitude ratio at 8 Hz vs. DOF. Each plot shows the magnitude ratios for an input in DOF i (row label) and output in DOF k (x-axis), which is the same as the magnitude ratios for an input in DOF k (x-axis) and output in DOF i (row label). These plots highlight which DOF are coupled, and that the magnitude ratios of proximal DOF (1-4) are smaller than those of distal DOF (5-7). The red circles present the magnitude ratios calculated using the full (coupled) matrices in Table 2.2, whereas the solid orange circles present the magnitude ratios calculated using only the diagonal (uncoupled) damping and stiffness matrices. The similarity between the red and orange circles demonstrates that the coupling is mostly due to inertia, not damping or stiffness.

Does tremor spread to all DOF, or does it focus in certain DOF? Tremor spreads in a relatively narrow manner: an input torque in a given DOF propagates mostly to a small subset of DOF (Figure 3.1D). Since the transfer matrix is symmetric (see Methods), the multiple-input case is easily predicted from the single-input case: the individual responses in a DOF due to (equal) inputs in all DOF are the same as the responses in all DOF due to an input in one DOF. For example, the responses in DOF 1-7 due to an input in DOF 1 are the same as the individual responses in DOF 1 due to inputs in DOF 1-7. Because an input in one DOF propagates mostly to a small subset of DOF, inputs in only some DOF significantly affect a given DOF. Consequently, simulations with inputs are not times more complicated than the single-input case. In fact, many of the responses are dominated by a single input, so for many DOF the response to inputs in all DOF is almost identical to the response to an input in the dominant DOF.

Does tremor propagation change from proximal to distal? There is a clear proximal-distal increase in the magnitude ratio (Figure 3.1D). Inputs in proximal DOF affect distal DOF equally or more (often much more) than proximal DOF. While the magnitude does not necessarily increase from DOF 5 to 7, one of these DOF always has the greatest magnitude ratio. In summary, there is more forward propagation than backward propagation. That said, note two caveats. First, even though there is more forward propagation than backward propagation, a distal input creates a bigger distal response than a proximal input of equal magnitude (compare scales in Figure 3.1C).

For example, an input in DOF 6 creates a bigger response in DOF 6 than an input in DOF 3 of equal magnitude. Second, a distal input creates a bigger proximal response than a proximal input of equal magnitude. For example, an input in DOF 6 creates a bigger response in DOF 3 than an (equal) input in DOF 3.

How does inertial loading affect tremor propagation? Increasing inertia produces competing trends; it decreases the natural frequency, shifting the magnitude ratio curve to the left, but it also decreases the damping ratio, raising the resonance peaks (Figure 3.2A). The end effect depends on frequency, but in the tremor band it usually decreases the magnitude ratio.

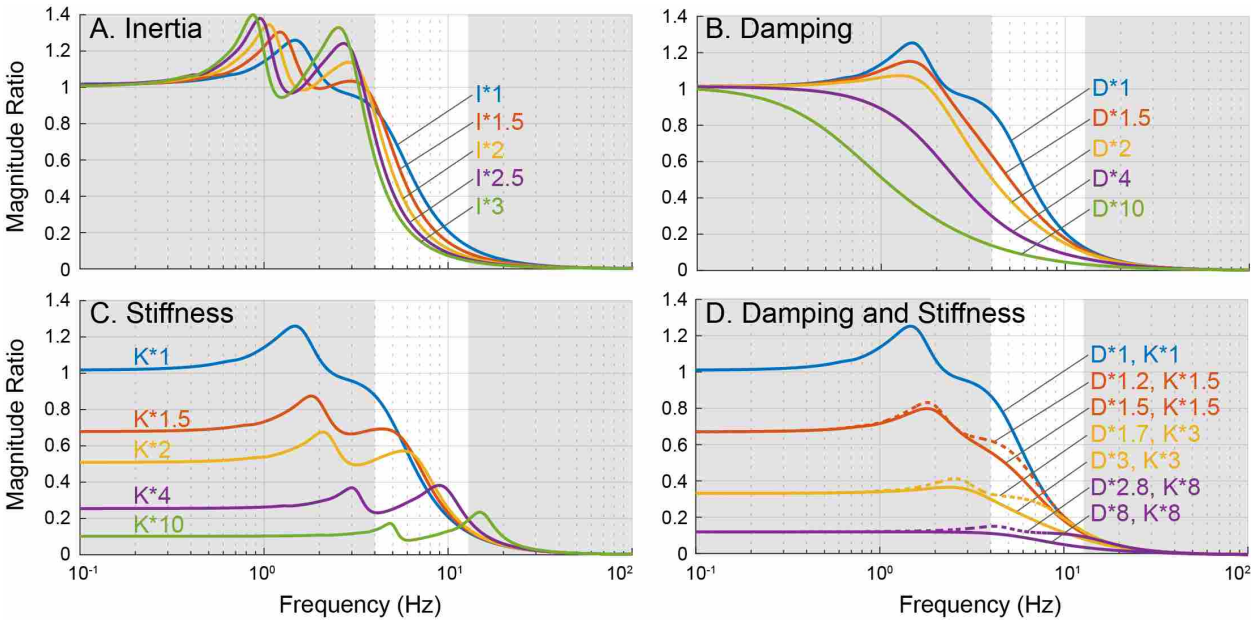

Figure 3.2: Effect of inertial and viscoelastic loading on the magnitude ratio, shown here for a representative input-output relationship (input and output in DOF 6). Although the magnitude ratios differ for different input-output relationships, the effect of inertial and viscoelastic loading is similar across relationships. In each plot, the default (no loading) is shown in blue. A. Increasing inertia usually decreases the magnitude ratio in the tremor band, though it can sometimes increase the magnitude ratio, especially at the lower bound of the tremor band (e.g. multiplying by 1.5 or 2 increases the magnitude ratio at 4 Hz). B. Increasing damping alone always decreases the magnitude ratio. C. Increasing stiffness alone can decrease or increase the magnitude ratio depending on the increase in stiffness and the input frequency. D. Increasing stiffness and damping by the same factor (solid lines) or stiffness more than damping (damping by the square root of the factor, dashed lines) usually decreases the magnitude ratio, but can increase the magnitude ratio for some factors and input frequencies.

How does viscoelastic loading affect tremor propagation? Increasing the damping, stiffness, or stiffness and damping together either decreased or increased the magnitude ratio, depending on the amount of increase and the tremor frequency (Table 3.1). Because increasing damping alone increased the damping ratio but had no effect on the natural frequency, it always decreased the magnitude ratio (Figure 3.2B). Increasing stiffness alone increased the natural frequency and decreased the damping ratio, shifting higher resonance peaks toward or into the tremor band, which raised the magnitude ratio (Figure 3.2C). However, increasing stiffness also decreased the DC gain, which lowered the magnitude ratio. The end effect depended on the amount of increase in stiffness and the tremor frequency. Increasing both damping and stiffness simultaneously by the same factor almost always decreased the magnitude ratio in the tremor band, especially for factors greater than 2.5 (Figure 3.2D). Likewise, increasing stiffness more than damping (by a factor and the square root of the factor, respectively, similar to co-contraction) usually decreased the magnitude ratio, but less robustly than increasing stiffness and damping by the same factor.

Table 3.1: Trends illustrating the effects of inertial and viscoelastic loading on the magnitude ratio. Increasing inertia (I), damping (D), and stiffness (K) directly affects the damping ratios (ζ), natural frequencies (ω_n), and DC gains. The combination of these competing effects dictate whether the magnitude ratio in the tremor band (M_{4-12Hz}) increases ($\uparrow$), decreases ($\downarrow$), or could do either depending on the amount of increase and the input frequency ($\uparrow\downarrow$). Stiffness and Damping refers to increasing both by the same factor, whereas Co-contraction refers to increasing stiffness by a factor and damping by the square root of that factor, similar to what occurs in co-contraction.

Simulation	I	D	K	ζ	ω_n	$DCgain$	M_{4-12Hz}
Inertia	$\uparrow$	-	-	$\downarrow$	$\downarrow$	-	$\uparrow\downarrow$
Damping	-	$\uparrow$	-	$\uparrow$	-	-	$\downarrow$
Stiffness	-	-	$\uparrow$	$\downarrow$	$\uparrow$	$\downarrow$	$\uparrow\downarrow$
Stiffness and Damping	-	$\uparrow$	$\uparrow$	$\uparrow$	$\uparrow$	$\downarrow$	$\uparrow\downarrow$
Co-contraction	-	$\uparrow$	$\uparrow$	-	$\uparrow$	$\downarrow$	$\uparrow\downarrow$

3.2 Sensitivity Analysis

3.2.1 Impedance Parameters

Errors in inertia, damping, and stiffness produce errors in the exact magnitude ratios, but the pattern of propagation remains relatively unchanged (Figure 3.3A-C). Multiplying inertia, damping, or stiffness matrices by factors ranging from 0.5 to 2 can have large effects on the magnitude ratios in individual DOF (as described above). However, for frequencies in the tremor band, the relative size of the magnitude ratios is quite unaffected. In particular, the statement that the three distal DOF exhibited the greatest magnitude ratios remained valid. The same is true for errors in the most sensitive elements of the matrices (I_{55}, D_{55}, K_{55}, D_{66}, K_{66}, I_{66}, K_{77}, D_{77}, all at 4 Hz). Multiplying these elements by 0.5 or 2 did not significantly alter the results because they affect the three distal DOF (5-7), each of which is dominated by a single phasor. Likewise, replacing the unknown off-diagonal values of the stiffness matrix (initially assumed zero) by non-zero values changed the magnitude ratios but not the coupling, even when the replacement values were very large (Figure 3.3D). The unknown off-diagonal elements in question couple the shoulder-elbow system to the forearm-wrist system. Replacing these elements with values as large as the diagonal elements creates unrealistically strong coupling. To clarify, coupling in the joint stiffness matrix reflects muscles that cross multiple DOF. Although coupling likely exists between some of the DOF in the two systems (such as elbow and forearm), it is unlikely to be as strong as the diagonal elements. In addition, many of the possible interactions between the shoulder-elbow and forearm-wrist systems are likely not coupled at all (e.g. shoulder flexion-extension and wrist flexion-extension). In summary, the propagation pattern was robust even when the unknown off-diagonal stiffness values were varied through an unrealistically large range. Finally, calculating the entire damping matrix using a single constant of proportionality did not significantly change the propagation pattern.

3.2.2 Posture Variation

Changing postures affected the coupling between DOF but not the proximal-distal increase in magnitude ratio (Figure 3.3E). Because coupling is mostly inertial, and because the inertia matrix is a function of posture, the coupling pattern greatly depends on posture. For example, in posture 1, DOF 4 and 7 have parallel axes and are therefore coupled, but pronating the forearm

by 90° rotates the axes of DOF 6 and 7 in a way that couples DOF 4 and 6 (instead of 4 and 7). The changes between postures 1-4 did not involve rotations of exactly 90° so coupling did not generally shift completely from one DOF to another. Nevertheless, the changes were large enough to significantly change the coupling pattern. That said, changes in posture that uncoupled some DOF usually coupled others, resulting in relatively little change in the total response in each DOF due to inputs in all DOF. In particular, the proximal-distal increase in magnitude ratio held true for all four postures.

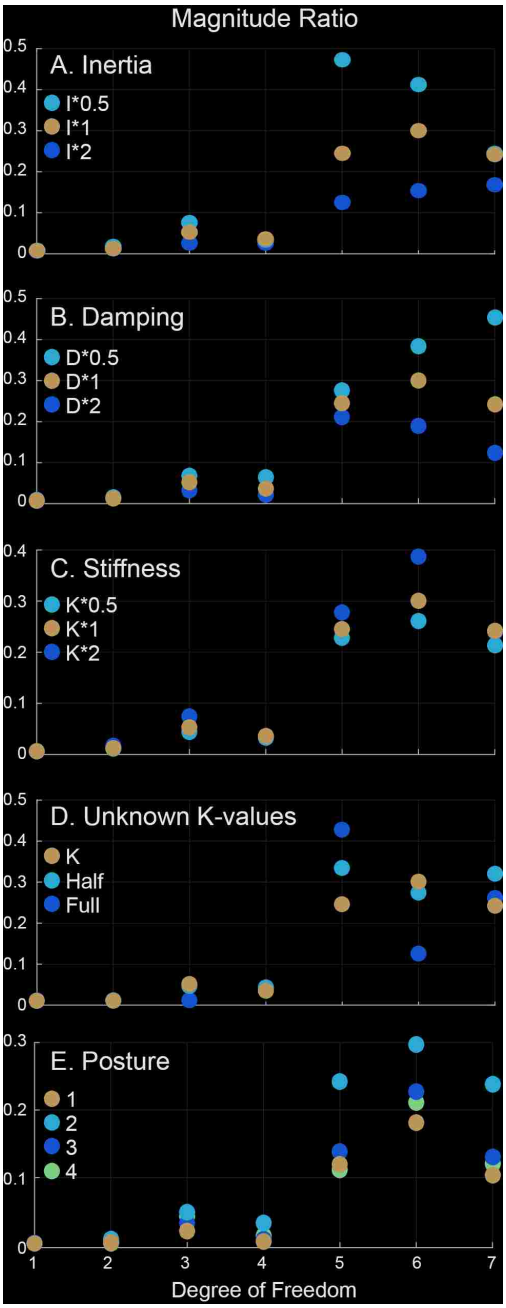

Figure 3.3: Sensitivity analysis results shown for the full multi-input multi-output case (magnitude ratio of the total output in each DOF for equal inputs in *all* DOF). Magnitude ratios were evaluated at 8 Hz. The blue magnitude ratios in each plot were calculated using the default inertia, damping, and stiffness matrices. A-C. Effect of multiplying inertia, damping, or stiffness by factors of 0.5 and 2 on the magnitude ratio. D. Effect of replacing the unknown off-diagonal values in the stiffness matrix (initially assumed zero) by half or the full average of the two corresponding diagonal values. E. Effect of posture. Changing posture tends to switch which DOF are coupled to each other (not shown), but the total amount of coupling in each DOF remains relatively unaffected.

CHAPTER 4. DISCUSSION

Here we present a basic analysis of tremor propagation to inform the future development of tremor suppressing devices. Optimally suppressing tremor requires a knowledge of the origin, propagation, and distribution of tremor throughout the upper limb. Here we present the first systematic investigation of how tremor propagates between the shoulder and the wrist. We deliberately implemented a simple model to focus first on the most basic (first-order) effects. From these first-order effects we have identified the following basic principles underlying the propagation of tremor in the upper limb. Note that these principles were observed under specific conditions (see Limitations below), and more research would be required to generalize outside of these conditions.

4.1 Principles of Simulated Tremor Propagation

Principle 1: Tremor is due in part to favorable limb dynamics. The magnitude of tremor depends on both the magnitude of the input torque and the magnitude ratio of the system at input frequency. More specifically, the magnitude of the tremor output is the product of the magnitude of the input torque and the magnitude ratio. Therefore, we conclude that tremor occurs most commonly over the 4-12 Hz band because this is the frequency band where the product of these two factors is greatest. This statement is obvious from the preceding sentence, but it demonstrates that the dynamics of the upper limb play a critical role in the magnitude of the tremor output. In other words, tremor is caused not only by a pathological input torque, but also by limb dynamics that favor the expression and propagation of tremor. In particular, the damping ratios of the upper limb are generally less than 0.707 [22, 28], resulting in resonance [30] in or near the tremor band. This in turn amplifies the effect of the input torque, creating larger tremor than there would be without resonance [4, 5]. As a corollary, there may be significant amounts of pathologically periodic input torque above the tremor band, but these input torques do not produce pathological tremor because the magnitude ratios at these frequencies are too small.

Principle 2: Tremor propagates mostly because of inertial coupling. Tremor propagates because the off-diagonal elements of the inertia, damping, and stiffness matrices couple the DOF. Most of this coupling is inertial, not viscoelastic; ignoring the off-diagonal elements of the stiffness and damping matrices has a minimal effect on the propagation pattern (Figure 3.1D). Note that this statement refers specifically to coupling, not whether inertial effects dominate the dynamics in general. To clarify, prior research showed a proximal-distal shift in the dominating impedance: whereas the dynamics of proximal joints (shoulder and elbow) are thought to be dominated by inertial effects, the dynamics of distal joints (wrist and forearm) are dominated by stiffness effects [10, 11]. However, this prior finding referred to the torques required to overcome the inertia, damping, and stiffness in a given DOF, not coupling between DOF. In addition, it referred to voluntary movements, which occupy a lower frequency band (mostly < 5 Hz [51]) than tremor (4-12 Hz), where inertial effects play a smaller role than at higher frequencies.

Principle 3: Tremor spreads narrowly. Although the inertia, damping, and stiffness matrices couple DOF to each other, some DOF are coupled only weakly or not at all. Consequently, input torque in a DOF significantly affects only a relatively small number of DOF. Because the transfer function matrix is symmetric, this also means that the vast majority of the tremor in a given DOF is due to inputs in a relatively small number of DOF (assuming equal input torques in all DOF). For example, although tremor in DOF 1 could be caused by a very large input torque in DOF 5, it is more easily caused by a smaller input torque in DOF 4 and/or 7. As stated in Principle 2, most of this coupling is inertial, which depends on posturetherefore, the pattern of coupling changes with posture (see Sensitivity Analysis).

Principle 4: Given equal amounts of input torque, the distal DOF have the greatest tremor magnitude. There is a clear increase in tremor magnitude from proximal to distal DOF of the upper limb; one of the three distal joints always has the largest magnitude ratio (Figure 3.1C and 3.1D). It appears this whip effect is caused by proximal-distal differences in impedance. Going from proximal to distal, inertia decreases more rapidly than stiffness (Figure 4.1). This creates a proximal-distal increase in the natural frequency, which pushes the resonance band to higher frequencies, elevating the magnitude ratios in the tremor band. While the shoulder and elbow can have higher magnitude ratios than the forearm and wrist DOF (Figure 3.1), their peaks are below the tremor band.

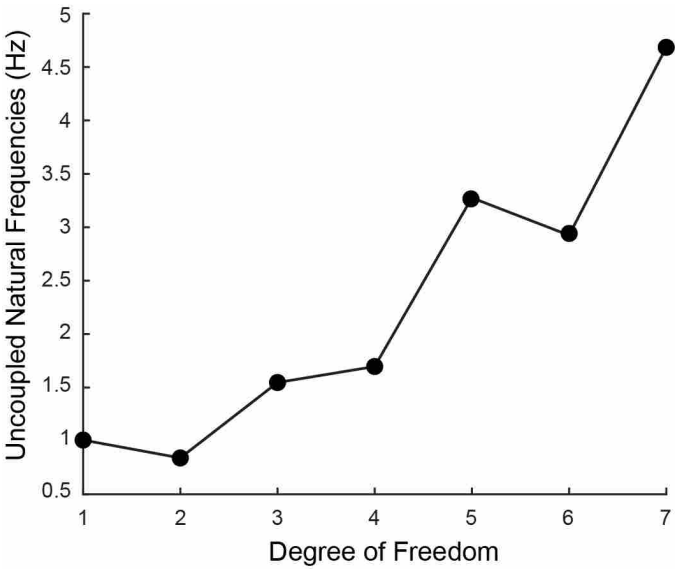

Figure 4.1: Uncoupled natural frequency at each DOF. These natural frequencies are proportional to the square root of stiffness over inertia. The proximal-distal increase in natural frequency demonstrates that the proximal-distal decrease in inertia is greater than the decrease in stiffness.

Principle 5: Increasing inertia can decrease or increase tremor. While increasing the inertia lowers the damping ratio, which raises resonant peaks, it also decreases the natural frequencies, which shifts the resonance peaks to lower frequencies and out of the tremor band. The most common end result in the tremor band is a decrease in magnitude ratio (Figure 3.2A). Most past experiments investigating inertial loading have measured a decrease in tremor [37, 39], and there exist a number of commercially available products (e.g. weighted utensils) that claim to mitigate tremor through weighting. However, recent studies have found that inertial loading does not always decrease tremor [40, 42], similar to our simulations. Note that these changes in magnitude ratio with inertial loading do not refer to the decrease in tremor frequency that can occur with inertial loading [37]–that phenomenon cannot be replicated by an LTI model with sinusoidal inputs, because in such a model the output frequency is always equal to the input frequency.

Principle 6: Increasing viscoelasticity can decrease or increase tremor. Increasing damping alone always decreased the magnitude ratio (Figure 3.2B), but increasing stiffness alone decreased or increased the magnitude ratio depending on the increase in stiffness and the frequency of the input (Figure 3.2C). Increasing stiffness and damping by the same factor almost always decreased tremor (Figure 3.2D). Therefore, efforts to develop braces (orthoses) that suppress tremor

must discern between stiffening schemes that do and those that do not decrease tremor. That said, effective braces could include properly designed increases in stiffness and/or inertia and do not need to rely solely on damping [52]. Increasing stiffness and damping with no change in the damping ratio (similar to co-contraction) also usually decreased tremor. Prior experiments similarly found that voluntary or artificially elicited muscle contractions attenuate the severity of tremor [2, 38].

4.2 Robustness of Principles

The principles presented are stable over the entire tremor band. Although the magnitude ratios often decrease significantly within the tremor band, the relative sizes of the magnitude ratios (comparing between DOF) remains relatively unaffected (Figure 3.1). Consequently, the principles are reasonably independent of tremor frequency.

The principles are also robust against physiologically plausible changes in impedance parameters. Although the tremor magnitudes depend on impedance parameters (Principles 5-6), the sensitivity analysis revealed that the principles were quite insensitive to relatively large changes in inertia, damping, or stiffness (Figure 3.3A-C), including changes in the unknown off-diagonal elements of the stiffness and damping matrices (Figure 3.3D) and changes in the constant of proportionality used to calculate the damping matrix. While variations in posture can change which DOF are coupled to each other, the principles are robust against the relatively large changes in postures tested here (Figure 3.3E).

In addition, transmission delay does not appear to have a significant effect on the propagation pattern. Our model assumed the torques in all DOF had the same phase despite differences in transmission delays which could affect the phase shifts between DOF and therefore the addition of individual outputs. We performed a rough estimate of the effect of including transmission delay on phase. Assuming that descending signals to wrist muscles travel 30 cm farther than signals to shoulder muscles, and that signals travel at an average speed of 30-50 m/s (which corresponds to short-latency finger reflex times of 30-50 ms round trip), the maximum phase shift is on the order of 10-25°, depending on travel speed and the frequency of the tremor (4-12 Hz). In other words, when adding phasors (Figure 3.1C), including transmission delays would rotate distal phasors by only about 10-25° relative to proximal phasors. This shift is too small to dramatically change

the vector sum (and therefore the total magnitude ratio), especially since almost all DOF have a dominant phasor that is much larger than the others, so rotating that phasor would not significantly change the magnitude of the vector sum, no matter how large the phase shift is.

4.3 Limitations

As mentioned above, we deliberately chose a simple model to establish the most basic, first-order effects. Our model is an LTI model of joint dynamics with realistic values of coupled inertia, damping, and stiffness. To analyze tremor propagation, we used the tools of frequency response, which focus on the steady-state response to sinusoidal inputs. We simulated tremor in a variety of postures away from the limits of the limbs range of motion. Therefore, our model ignores the following factors: non-sinusoidal torque inputs, non-linear dynamics, time-varying impedance parameters, reflexes, gravity, kinetic tremor (tremor during movement), transient responses, and effects that occur close to the end of the range of motion (e.g. when the arm is fully extended). Future studies should characterize how these factors affect tremor propagation, especially the basic principles established here.

Our simulations assumed equal input torques. For the multiple-input case, we assumed the torque inputs in different DOF had equal amplitude, frequency, and phase. The amplitudes are most likely not equal, but assuming equal amplitudes allows comparison on an equal footing. The assumption of equal frequency is reasonable—there is no evidence of different frequencies in different DOF. Likewise, the assumption of equal phase is reasonable since the effect of phase delay between DOF is small because most DOF have a dominant phasor.

Finally, our principles are based on simulations and were not validated by comparison to experimentally observed tremor propagation patterns. To the best of our knowledge, there do not exist prior measurements of how tremor propagates throughout the upper limb. The availability of in vivo measurements of tremor propagation patterns would allow one to identify elements of actual tremor reproduced by our simple model (and therefore likely caused by one of the first-order effects included in our model), and those that were not reproduced by our simple model (and therefore likely caused by higher-order effects).

4.4 Conclusion

Using a simple model of musculoskeletal dynamics, we have established six basic principles underlying the propagation of tremor in the upper limb. Our principles agree with prior experimental studies investigating the effects of inertial loading and co-contraction on tremor magnitude. The principles were shown to be stable over the frequency band of most tremors and quite robust against many physiologically plausible variations in joint impedance. This work has been submitted to a journal for publication and we expect that these principles will serve as a foundation for more sophisticated models of tremor propagation and for the development of tremor-suppressing devices.

REFERENCES

[1] Anouti, A., and Koller, W. C., 1995. "Tremor disorders. Diagnosis and management." *Western journal of medicine,* **162**(6), p. 510. 1

[2] Gallego, J. Á., Rocon, E., Belda-Lois, J. M., and Pons, J. L., 2013. "A neuroprosthesis for tremor management through the control of muscle co-contraction." *Journal of NeuroEngineering and Rehabilitation,* **10**(1), pp. 1–13. 1, 11, 25

[3] Hellwig, B., Haussler, S., Schelter, B., Lauk, M., Guschlbauer, B., Timmer, J., and Lucking, C. H., 2001. "Tremor-correlated cortical activity in essential tremor." *Lancet,* **357**(9255), pp. 519–523. 1

[4] Lakie, M., Vernooij, C. A., Osler, C. J., Stevenson, A. T., Scott, J. P. R., and Reynolds, R. F., 2015. "Increased gravitational force reveals the mechanical, resonant nature of physiological tremor." *The Journal of physiology,* **593**(19), pp. 4411–4422. 1, 22

[5] Lakie, M., Vernooij, C. A., Osborne, T. M., and Reynolds, R. F., 2012. "The resonant component of human physiological hand tremor is altered by slow voluntary movements." *The Journal of physiology,* **590**(10), pp. 2471–2483. 1, 22

[6] Rocon, E., Belda-Lois, J. M., Sanchez-Lacuesta, J. J., and Pons, J. L., 2004. "Pathological tremor management: Modelling, compensatory technology and evaluation." *Technology & Disability,* **16**(1), pp. 3–18. 1

[7] Elble, R. J., and Deuschl, G., 2009. "An update on essential tremor." *Current Neurology and Neuroscience Reports,* **9**(4), pp. 273–277. 1

[8] Zesiewicz, T. A., Elble, R., Louis, E. D., Hauser, R. A., Sullivan, K. L., Dewey, R. B., Ondo, W. G., Gronseth, G. S., and Weiner, W. J., 2005. "Practice parameter: Therapies for essential tremor - Report of the quality standards subcommittee of the American Academy of Neurology." *Neurology,* **64**(12), pp. 2008–2020. 1

[9] Heldman, D. A., Jankovic, J., Vaillancourt, D. E., Prodoehl, J., Elble, R. J., and Giuffrida, J. P., 2011. "Essential tremor quantification during activities of daily living." *Parkinsonism Related Disorders,* **17**(7), pp. 537–542. 1

[10] Charles, S. K., and Hogan, N., 2011. "Dynamics of wrist rotations." *Journal of Biomechanics,* **44**(4), pp. 614–621. 3, 23

[11] Peaden, A. W., and Charles, S. K., 2014. "Dynamics of wrist and forearm rotations." *Journal of Biomechanics,* **47**(11), pp. 2779–2785. 3, 23

[12] De Leva, P., 1996. "Adjustments to zatsiorsky-seluyanov's segment inertia parameters." *Journal of Biomechanics,* **29**(9), pp. 1223–1230. 6

[13] Corke, P., 2011. *Robotics, Vision and Control: Fundamental Algorithms in MATLAB.*, Vol. 73 Springer. 6

[14] Spong, M. W., Hutchinson, S., and Vidyasagar, M., 2006. *Robot Modeling and Control*. John Wiley Sons, Inc, Hoboken, NJ. 6

[15] Gomi, H., and Osu, R., 1998. "Task-dependent viscoelasticity of human multijoint arm and its spatial characteristics for interaction with environments." *Journal of Neuroscience,* **18**(21), pp. 8965–8978. 6, 12

[16] Lipps, D. B., Baillargeon, E. M., Ludvig, D., and Perreault, E. J., 2015. "System Identification of Multidimensional Shoulder Impedance During Volitional Contractions." *IFAC-PapersOnLine,* **48**(28), pp. 1369–1374. 6

[17] Pando, A. L., Lee, H., Drake, W. B., Hogan, N., and Charles, S. K., 2014. "Position-dependent characterization of passive wrist stiffness." *IEEE Transactions on Biomedical Engineering,* **61**(8), pp. 2235–2244. 6, 9

[18] Formica, D., Charles, S. K., Zollo, L., Guglielmelli, E., Hogan, N., and Krebs, H. I., 2012. "The Passive Stiffness of the Wrist and Forearm." *Journal of Neurophysiology,* **108**, pp. 1158–1166. 6, 9

[19] Hogan, N., 1985. "The Mechanics of Multi-Joint Posture and Movement Control." *Biological Cybernetics,* **52**, pp. 315–331. 6, 9

[20] Drake, W. B., and Charles, S. K., 2014. "Passive stiffness of coupled wrist and forearm rotations." *Annals of Biomedical Engineering,* **42**(9), pp. 1853–1866. 6

[21] Dolan, J. M., Friedman, M. B., and Nagurka, M. L., 1993. "Dynamic and Loaded Impedance Components in the Maintenance of Human Arm Posture." *Ieee Transactions on Systems Man and Cybernetics,* **23**(3), pp. 698–709. 6

[22] Perreault, E. J., Kirsch, R. F., and Crago, P. E., 2004. "Multijoint dynamics and postural stability of the human arm." *Experimental Brain Research,* **157**(4), pp. 507–517. 6, 7, 12, 22

[23] Tsuji, T., Morasso, P. G., Goto, K., and Ito, K., 1995. "Human Hand Impedance Characteristics During Maintained Posture." *Biological Cybernetics,* **72**(6), pp. 475–485. 6

[24] Charles, S. K., and Hogan, N., 2012. "Stiffness, not inertial coupling, determines path curvature of wrist motions." *Journal of Neurophysiology,* **107**(4), pp. 1230–1240. 6, 11

[25] Salmond, L. H., Davidson, A., and Charles, S. K. I. r. "Proximal-Distal Differences in Movement Smoothness Reflect Differences in Biomechanics.". 6, 11

[26] Halaki, M., O'Dwyer, N., and Cathers, I., 2006. "Systematic nonlinear relations between displacement amplitude and joint mechanics at the human wrist." *Journal of Biomechanics,* **39**(12), pp. 2171–2182. 7

[27] Lakie, M., Walsh, E. G., and Wright, G. W., 1984. "Passive wrist movements - thixotropy - measurement of memory time." *Journal of Physiology-London,* **346**(JAN), pp. P6–P6. 7

[28] Sinkjaer, T., and Hayashi, R., 1989. "Regulation of wrist stiffness by the stretch reflex." *Journal of Biomechanics,* **22**(11-12), pp. 1133–1140. 7, 22

[29] Dijkstra, E. J., 2010. "Upper limb project.". 7

[30] Palm, W., 2014. *System Dynamics*., 3rd ed. McGraw Hill, New York, NY. 9, 10, 22

[31] Goldstein, H., Poole, C., and Safko, J., 2002. *Classical Mechanics*., 3rd ed. Addison Wesley, San Francisco, CA. 9

[32] Levine, W. S., 2010. *The Control Handbook: Control System Fundamentals*. CRC Press. 10

[33] Smith, J., 2007. *Introduction to Digital Filters with Audio Applications*. W3K Publishing. 10

[34] Deuschl, G., Bain, P., and Brin, M., 1998. "Consensus statement of the movement disorder society on tremor. Ad Hoc Scientific Committee." *Mov Disord,* **13**. 11

[35] Aisen, M. L., Arnold, A., Baiges, I., Maxwell, S., and Rosen, M., 1993. "The effect of mechanical damping loads on disabling action tremor." *Neurol,* **43**. 11

[36] Dahlin-Webb, S. R., 1986. "A Weighted Wrist Cuff." *Am J Occup Ther,* **40**(5), pp. 363–364. 11

[37] Elble, R. J., 1986. "Physiologic and essential tremor." *Neurology,* **36**(2), pp. 225–231. 11, 24

[38] Heroux, M. E., Pari, G., and Norman, K. E., 2010. "The effect of contraction intensity on force fluctuations and motor unit entrainment in individuals with essential tremor." *Clinical Neurophysiology,* **121**(2), pp. 233–239. 11, 25

[39] Hewer, R. L., Cooper, R., and Morgan, M. H., 1972. "An investigation into the value of treating intention tremor by weighting the affected limb." *Brain,* **95**. 11, 24

[40] Ma, H.-I., Hwang, W.-J., Tsai, P.-L., and Hsu, Y.-W., 2009. "The effect of eating utensil weight on functional arm movement in people with Parkinson's disease: a controlled clinical trial." *Clinical rehabilitation,* **23**(12), pp. 1086–1092. 11, 24

[41] McGruder, J., Cors, D., Tiernan, A. M., and Tomlin, G., 2003. "Weighted wrist cuffs for tremor reduction during eating in adults with static brain lesions." *American Journal of Occupational Therapy,* **57**(5), pp. 507–516. 11

[42] Meshack, R. P., and Norman, K. E., 2002. "A randomized controlled trial of the effects of weights on amplitude and frequency of postural hand tremor in people with Parkinson's disease." *Clinical rehabilitation,* **16**(5), pp. 481–492. 11, 24

[43] Pledgie, S., Barner, K. E., Agrawal, S. K., and Rahman, T., 2000. "Tremor suppression through impedance control." *IEEE Trans Rehabil Eng,* **8**. 11

[44] Seegmiller, D. B., and Charles, S. K. I. p. "Common wrist orthoses and their effects on the stiffness of wrist rotations." *Journal of Rehabilitation Research and Development*. 12

[45] De Serres, S. J., and Milner, T. E., 1991. "Wrist muscle activation patterns and stiffness associated with stable and unstable mechanical loads." *Experimental Brain Research,* **86**, pp. 451–458. 12

[46] de Vlugt, E., van Eesbeek, S., Baines, P., Hilte, J., Meskers, C. G. M., and de Groot, J. H., 2011. "Short range stiffness elastic limit depends on joint velocity." *Journal of Biomechanics,* **44**(11), pp. 2106–2112. 12

[47] Klomp, A., de Groot, J. H., de Vlugt, E., Meskers, C. G. M., Arendzen, J. H., and van der Helm, F. C. T., 2014. "Perturbation Amplitude Affects Linearly Estimated Neuromechanical Wrist Joint Properties." *Ieee Transactions on Biomedical Engineering,* **61**(4). 12

[48] Colacino, F. M., Rustighi, E., and Mace, B. R., 2012. "Subject-specific musculoskeletal parameters of wrist flexors and extensors estimated by an emg-driven musculoskeletal model." *Medical Engineering Physics,* **34**(5), pp. 531–540. 12

[49] Hu, X., Murray, W. M., and Perreault, E. J., 2011. "Muscle short-range stiffness can be used to estimate the endpoint stiffness of the human arm." *J Neurophysiol,* **105**(4), pp. 1633–1641. 13

[50] Perreault, E. J., Kirsch, R. F., and Crago, P. E., 2001. "Effects of voluntary force generation on the elastic components of endpoint stiffness." *Experimental Brain Research,* **141**(3), pp. 312–323. 13

[51] Mann, K. A., Werner, F. W., and Palmer, A. K., 1989. "Frequency-Spectrum Analysis of Wrist Motion for Activities of Daily Living." *Journal of Orthopaedic Research,* **7**(2), pp. 304–306. 23

[52] Kotovsky, J., and Rosen, M. J., 1998. "A wearable tremor-suppression orthosis." *Journal of Rehabilitation Research and Development,* **35**(4), pp. 373–387. 25